日本機械学会流体工学部門講演会講演論文集 (2001.10.2-3・蔵王)

Numerical Simulation on the Flow Field around Turbine Nozzle Vanes with Upstream Flow Injection from the Outer Casing

Ken-ichi FUNAZAKI, Iwate University, Ueda 4-3-5, Morioka, 020-0066
Carlos Felipe Ferreira FAVARETTO, Iwate University, Ueda 4-3-5, Morioka, 020-0066
Tadashi TANUMA, Toshiba Corporation, Keihin Product Operations, Tsurumi-Ku, Yokohama, 230-0045

A steady three-dimensional numerical simulation of the flow field inside turbine nozzle vanes is presented. Two different types of geometry were analyzed: unleaned blade and 5^0 positively leaned blade. The calculations were performed considering the no injection case and 5% main stream flow injection from the outer casing. The paper presents an investigation of the effects of the blade lean and the upstream air injection from the outer casing on the aerodynamic loss in terms of the energy loss coefficient.

Key Words: *Inlet Distortion, Flow Injection, Turbine Nozzle, Leaned Blade*

1. INTRODUCTION

In some combined cycle steam turbines, injection flows (from 5 to 15% of main mass flow rate) from steam generators are induced between turbine stages.

The upstream steam injected from the outer casing is usually at a different temperature and velocity than the main flow. The mixing phenomena of the injected steam and the main flow generates secondary flow fields and pressure losses resulting in inlet flow distortion upstream the stator (Fig.1). This distortion will generate pitchwise and spanwise variations of the mass flow and the unsteadiness of the inlet flow angle. Such variation will change the turbine stage operating conditions, affecting the blading flow pattern and efficiency.

Due to the lack of information on the flow field generated by the flow distortion and the increasing demand of the steam turbine companies in designing high performance machines, a remarkable number of authors have been investigating the phenomena by applying numerical simulation or performing experimental analysis.

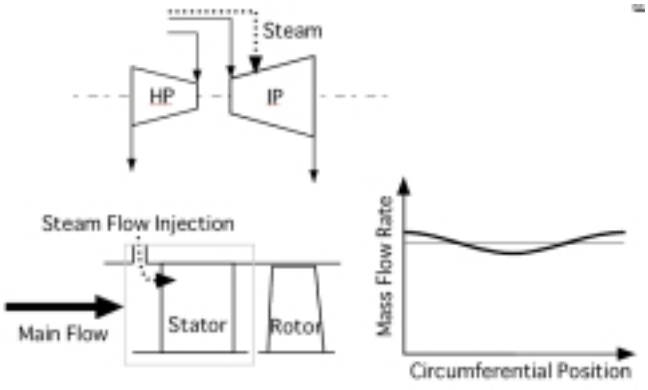

Fig. 1: Flow Injection Schematic Diagram.

In the work of Hirai et al.[1], numerical simulation was used to investigate the effect of circumferential positions of inlet hot streaks to a single stage turbine. The pressure loss due to unsteady flow for a transonic rotor with inlet total pressure distortion was also analyzed. Adamczyk[2] outlined the unsteady aerodynamic interaction effects on turbomachinery blade life and performance.

Moser[3] investigated distorted flow conditions caused by asymmetric exhaust and by ribs in the radial and circumferential direction by using pneumatic probes. Zeschky and Gallus[4] determined the effects of the outlet distortion provided from the stator exit on the turbine rotor by using three-dimensional hot-wire and pneumatic probes. The formation of the passage vortices in the rotor were found to be strongly influenced by the nonuniform stator outlet flow which caused the accumulation of low-energy fluid in the rotor wake close to midspan.

In order to minimize the loss effects caused by the flow distortion several design techniques have been developed. For instance, Harvey et al.[5] proposed a linear design system which generates end wall nonaxisymmetric profiles in order to reduce secondary flows, in particular secondary kinetic energy and exit angle deviations. The final profiled hub wall design presented in the paper showed a reduction of the size of the passage vortex, decreasing the loss for almost one quarter of the blade span.

Other design techniques which can be comparable to the nonaxisymmetric profile are blade leaning, skewing and bowing (compound lean). Harrison[6] presented a study on the actual contribution of the blade lean on the reduction of the loss coefficient. It was found that simple lean reduces velocities and loss generation substantially at one end wall and increases them at the opposite wall. Compound lean reduced the enwall and downstream mixing losses, increased the flow turning and substantially reduced spanwise variations on the span angle.

Songtao et al.[7] performed a similar study considering two bow angles. It was shown that although blades with positively bow angle can decrease the endwall loss, the midspan loss will increase.

In the present study, the influence of the lean angle on the aerodynamic performance of a turbine nozzle vane was analyzed. Initially, a comparison between a leaned and unleaned vane with no flow injection was performed. Following this analysis, the influence of the blade lean for a distorted inlet flow was evaluated.

2. METHODOLOGY

Numerical simulation was performed considering two types of turbine nozzle vanes (Fig.2): unleaned blade (*case A*) and 5^0 positively leaned blade (*case B*). Initially, no flow injection was considered and the results for *case A* were compared to the experimental data.

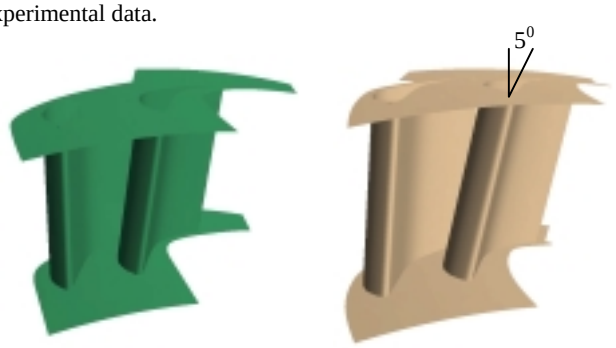

Fig. 2: Unleaned and 5^0 positively leaned nozzle vanes.

Once the boundary conditions and the flow quantities were validated, calculations were performed for *case B*. In order to analyze the flow distortion effects, flow injection from the outer casing was added to the computational domain and simulations were carried out for the unleaned (*case C*) and leaned (*case D*) nozzle vanes.

In order to enable a comparison of the numerical results with the experimental data the main stream fluid as well as the injected fluid were considered as air.

3. NUMERICAL SIMULATION

3.1 Grid Generation

A structured multi-block grid system was generated with the *CFX-TurboGrid 1.0* software. For the analysis cases where no injection effects were modeled, the computational domain consisted of one O-type grid block surrounding the blade (*MAIN*), one C-type grid block around the O-type grid from the inlet region to the trailing edge (*CGRID*) and two H-type grid blocks (*TEDPS* and *TEDSS*) extending from the trailing edge to the outlet region on the pressure and suction sides.

For the cases where the flow was injected from the outer casing, an additional H-type grid block (*INBLOCK*) was necessary to enable a more representative discretization of the domain. Table 1 indicates the grid system configuration adopted for each one of the analyzed cases.

	No air injection		Air injection	
	Case A (unleaned)	Case B (leaned)	Case C (unleaned)	Case D (leaned)
MAIN	166x17x50	211x17x50	166x17x50	211x17x50
CGRID	111x16x50	151x21x50	111x16x50	151x21x50
TEDPS	71x31x50	86x31x50	71x31x50	86x31x50
TEDSS	31x31x50	36x31x50	31x31x50	36x31x50
INBLOCK	-	-	16x11x50	16x11x50

Table 1: Grid system for the analyzed cases.

3.2 Computational Code

The three-dimensional, steady-state, Reynolds-averaged, compressible Navier-Stokes equations were solved with the *CFX-TASCflow 2.10.0* computational code. Several numerical analyses of the flow field inside turbomachinery were performed by using this code, as described in von Hoyningen–Huene and Hermeler[8] and Favaretto[9].

Concerning the domain discretization, the code uses a finite volume method based on the finite elements method in order to enable a more accurate modeling of the geometry. The diffusive terms are calculated by the conventional finite elements method using shape functions to calculate the derivatives. In the same fashion, the pressure gradient terms in the momentum equations are also determined.

For the advective terms, a second-order *UDS* (Upwind Differencing Scheme) was employed. The solution algorithm uses the *AMG* (Algebraic Multigrid) method which is based on the *ACM* (Additive Correction Method) correction strategy. The algorithm is fully coupled, ie. the momentum and continuity equations are solved simultaneously. The unstructured data structure allows connectivities in periodicity and grid interface regions to be solved in a fully implicit fashion. Detailed information on the theoretical basis of the software can be found in the CFX-TASCflow Theory Documentation[10].

3.3 Boundary Conditions

The boundary conditions employed were based on the experimental data. For the inlet region, total pressure, total temperature, flow angle, inlet turbulence intensity (5%) and inlet eddy length scale (0.05m) were prescribed. For the outlet region, static pressure was prescribed. Concerning cases *C* and *D*, an additional inlet region was added to model the flow injection. In this region, the velocity was prescribed normal to the outer casing and its magnitude was calculated as 5% of the main stream flowrate (Fig.3). The same value for the total temperature at the inlet was prescribed in the flow injection region. The average Reynolds number for all cases was 550,000.

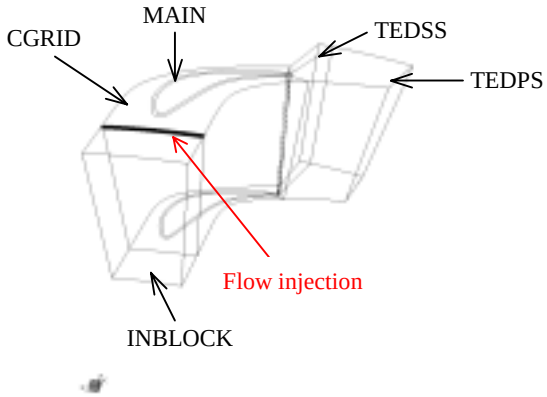

Fig. 3: Grid block configuration (*case C* – unleaned, air injection).

The blade, hub and tip wall regions were assumed as adiabatic and the non-slip condition was applied. A logarithm wall function was used for the near-wall grid points. For the pitchwise boundaries, periodic boundary condition was applied.

3.4 Turbulence Model

Due to the highly turbulent region behind the trailing edge, where the flow must be regarded as non-isotropic, the Reynolds stress second-order closure turbulence model was employed. In addition to the anisotropic turbulence calculation feature, the model can solve the production term without any modeling.

3.5 Initial Values

The computational code prints the global length, time and flow property scales before the solution process begins in order to assist the user on the time step and flow quantity initial value estimation. Thus, the time step adopted was 0.0005 s and the initial values were: u = 34 m/s, v = 0 m/s, w = 0 m/s, T = 344 K, P = 0.145 MPa, eddy length scale = 0.05 m and turbulence intensity of 5%. The initial values for the turbulent kinetic energy

and the dissipation of the turbulent kinetic energy were calculated from the turbulence intensity and eddy length scale. The turbulent viscosity was initialized from the turbulent kinetic energy and the dissipation of the turbulent kinetic energy fields. The Reynolds stress tensor terms were initialized to zero.

3.6 Convergence Analysis

The calculations were performed in the Silicon Graphics Origin 3400 machine at Iwate University Computing Center using single processing. After running 150 iterations the normalized residuals were smaller than 10^{-6} for the four cases analyzed. The CPU time was approximately 60,000 s for cases *A* and *C* and 80,000 s for cases *B* and *D*.

4. RESULTS

4.1 No Air Injection (Cases A and B)

Figs. 4 and 5 present the normalized static pressure distribution on the blade surface at the hub and tip for cases *A* and *B*. The results were normalized in terms of the inlet total pressure.

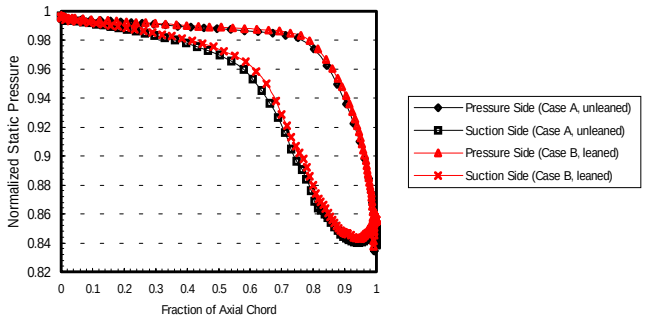

Fig. 4: Normalized Static Pressure Distribution on the Blade Surface (Hub).

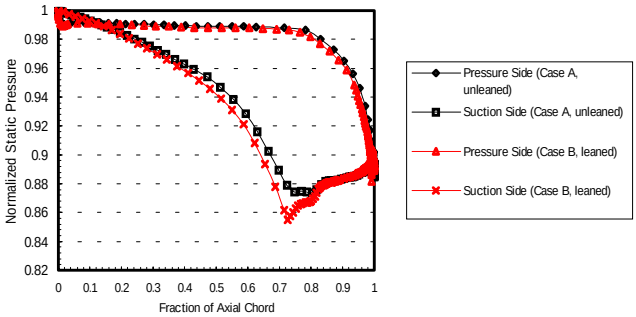

Fig. 5: Normalized Static Pressure Distribution on the Blade Surface (Tip).

Considering the pressure difference from the pressure side to suction side (crossflow pressure gradient) at the hub, one can find a decrease for the leaned blade case (case *B*) in the range of approximately 40% to 80% of the axial chord. For the tip (Fig.5), however, the crossflow pressure gradient was increased for case *B*.

The results obtained show that the blade lean can decrease the crossflow pressure gradient near the hub which may decrease the passage vortex strength and reduce the secondary loss near the wall. On the other hand, the crossflow pressure gradient is increased at the hub suggesting that there must be an optimum value for the lean angle in order to balance the gain and loss.

Fig.6 presents the pitchwisely masss-averaged normalized energy loss coefficient (JSME[11]) for the no injected flow cases (Eq.1).

$$\xi = \frac{\left(P_{01}/P_{02}\right)^{\frac{\gamma-1}{\gamma}} - 1}{\left(P_{01}/P_{2}\right)^{\frac{\gamma-1}{\gamma}} - 1} \qquad (1)$$

where: ξ is the energy loss coefficient, P_{01} the inlet total pressure, P_{02} the outlet total pressure, P_2 the outlet static pressure and γ the specific heat ratio.

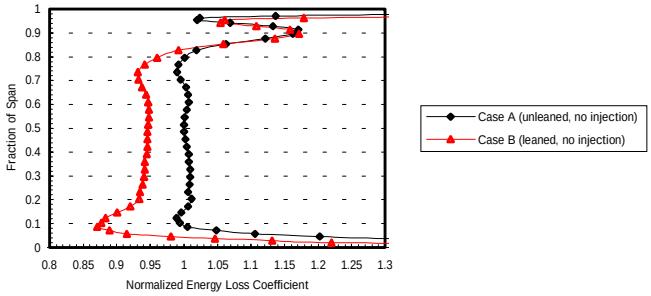

Fig. 6: Normalized Pitchwisely Mass-averaged Energy Loss Coefficient.

The results from Fig.6, normalized by the value of case *A* at midspan, indicate that the reduction in the pressure loss coefficient obtained with the leaned blade extends from the hub to almost 85% span. In the midspan the reduction in loss was approximately 5% whereas at 10% percent span the maximum difference of 12% was obtained. An increase in loss can be barely seen from 90% span to the tip.

4.2 Air Injection (Cases C and D)

Fig.7 shows the velocity vectors obtained for the unleaned nozzle vane with air injection. The disturbance on the main flow due to the injection affected approximately 30% span from the tip. A vortex was formed due to the low energy fluid accumulated close to the wall. This vortex extends along the whole pitchwise direction since the main flow inlet boundary condition is axisymmetric as well as the injected flow.

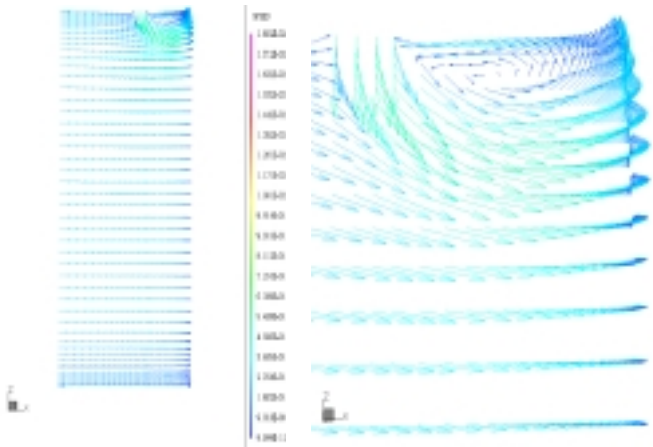

a – Plane at 50% pitch (from the inlet to leading edge).

b – Magnified view of the velocity vector plot.

Fig. 7: Velocity Vectors (unleaned blade).

The normalized static pressure distribution on the blade surface for cases *C* and *D* is shown in Figs. 8 and 9. The same remarks made for cases *A* and *B* may be considered here, ie. the crossflow pressure gradient was decreased for the leaned nozzle vane.

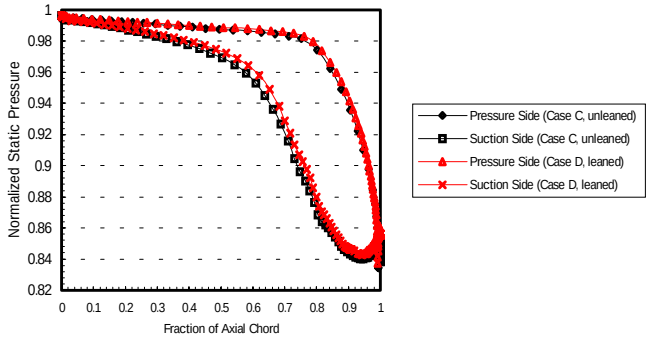

Fig. 8: Normalized Static Pressure Distribution on the Blade Surface (Hub).

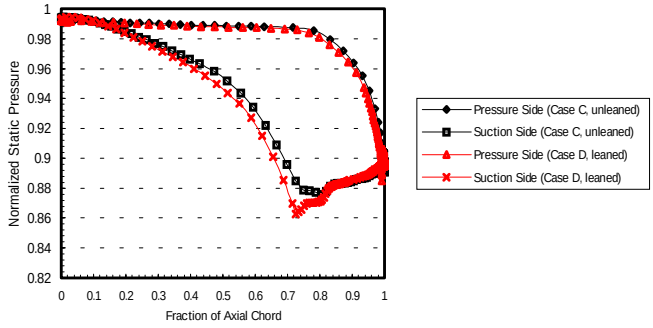

Fig. 9: Normalized Static Pressure Distribution on the Blade Surface (Tip).

The energy loss coefficient for cases *C* and *D* was also calculated by Eq.1, but the inlet total pressure term (P_{01}) was evaluated at the interface between the INBLOCK and the CGRID blocks. Without such assumption, the actual loss effects may not be taken into account since the boundary conditions at the inlet region were the same as in cases *A* and *B*.

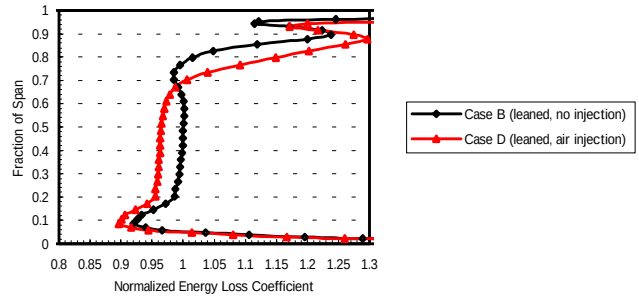

Fig. 10: Normalized Pitchwisely Mass-averaged Energy Loss Coefficient.

Fig.10 presents the normalized energy loss coefficient distribution in the pitchwise direction for cases *B* and *D*. The loss effects due to the air injection can be seen from 70% span to the tip. No significant loss increase can be found for the other regions in the spanwise direction.

In Fig.11 a comparison between the unleaned and the leaned nozzle vane energy loss coefficient is presented. As expected from case *B*, the decrease in loss extends from the hub to 85% span, being more significant in the region near the hub (9% span) where the maximum difference obtained was 15%.

Considering the region affected by the air injection extending from approximately 70% span to the tip, the positively leaned blade can reduce the loss even though in a lower magnitude than in the midspan and near-hub regions.

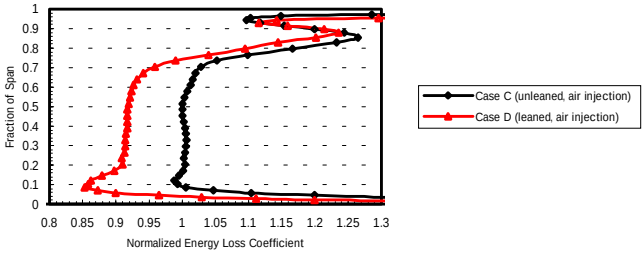

Fig. 11: Normalized Pitchwisely Mass-averaged Energy Loss Coefficient.

5. CONCLUSIONS

A numerical analysis of the flow field in turbine nozzle vanes was performed. The first two cases analyzed, unleaned and leaned nozzle vanes with no air injection, enabled a better understanding of the blade lean effects on the energy loss. The leaned blade presented reduced crossflow pressure gradient at the hub and increased values at the tip. The energy loss coefficient was also reduced from the hub to approximately 85% span.

The air injection effects caused a disturbance on the flow from the tip to around 70% span. The leaned blade caused a loss reduction from the hub to 85% span. The results show that the reduction in loss for the disturbed region were not very significant since the blade is positively leaned.

The computational code presented satisfactory results for the present analysis. The authors foresee the necessity of continuing the present research in order to obtain a more optimized nozzle vane for a larger span range.

References

(1) Hirai, K., Kodama, H., Nozaki, O., Kikuchi, K., Tamura, A., Matsuo, Y., 1997. Unsteady Three-Dimensional Analysis of Inlet Distortion in Turbomachinery. AIAA Paper 97-2735.

(2) Adamczyk, J.J., 1992. Unsteady Aerodynamic Interaction Effects on Turbomachinery Blade Life and Performance. AIAA Paper 92-0149.

(3) Moser, W., 1989. An Analysis of Outlet Distortion in LP Steam Turbines. ASME Paper 89-GT-237.

(4) Zeschky, J., Gallus, H.E., 1993. Effects of Stator Wakes and Spanwise Nonuniform Inlet Conditions on the Rotor Flow of an Axial Turbine Stage. ASME Journal of Turbomachinery, Vol. 115, pp. 128-136.

(5) Harvey, N.W., 2000. Nonaxisymmetric Turbine End Wall Design: Part I – Three-Dimensional Linear Design System. ASME Journal of Turbomachinery, Vol. 122, pp. 278-285.

(6) Harrison, S., 1992. The Influence of Blade Lean on Turbine Losses. ASME Journal of Turbomachinery, Vol. 114, pp. 184-190.

(7) Songtao, W., Zhongqi, W., Guotai, F., 2001. Numerical Simulation of 3D Flow Field Structure in Turbine Cascade with Bowed Blades. ASME Paper 2001-GT-0442.

(8) von Hoyningen-Huene, M., Hermeler, J., 1999. Time-Resolved Numerical Analysis of the 2-D Aerodynamics in the First Stage of an Industrial Gas Turbine for Different Vane-Blade Spacings", ASME Paper 99-GT-102

(9) Favaretto, C.F.F., 2000. Análise dos Efeitos Dinâmicos e Cinemáticos numa Turbina de Medição. MSc Thesis, Federal University of Rio Grande do Sul (UFRGS), Porto Alegre, Brazil.

(10) CFX-TASCflow Theory Documentation, 2000. AEA Technology Engineering Software Ltd., Version 2.10, Waterloo, Ontario, Canada.

(11) JSME Data Book: Flow Measurements, July 1985, JSME.